Silicon
https://doi.org/10.1007/s12633-017-9698-7

ORIGINAL PAPER

Effect of Si and Ge Surface Doping on the Be_2C Monolayer: Case Study on Electrical and Optical Properties

Mosayeb Naseri[1] · Ali H. Reshak[2,3] · Arash Boochani[1] · D. P. Rai[4] · Laleh Farhang Matin[5] · Shahram Solaymani[6]

Received: 1 January 2017 / Accepted: 23 November 2017
© Springer Science+Business Media B.V., part of Springer Nature 2018

Abstract
The electronic and optical properties of X (Si, Ge) doped Be_2C monolayer has been investigated using the all-electron full potential linear augmented plane wave (FP-LAPW+lo) method in a scalar relativistic version as embodied in the Wien2k code based on the density functional theory. Using cohesive energy calculation, it has been shown that the Si and Ge doped to Be_2C monolayer have stable structures and the doping processes modified the direct band gaps. The calculated electronic band structure confirm the direct band gap nature since the conduction band minimum and the valence band maximum are located at the center of the Brillouin zone. The total and partial density of states help to gain further information regarding the hybridizations and the orbitals which control the energy band gap. The calculated optical properties help to gain deep insight into the electronic structure. Our calculated results indicate that the X (Si, Ge) doped Be_2C monolayer can be have potential application in optoelectronics devices.

Keywords Be_2C monolayer · Electrical properties · Optical properties · DFT calculations

1 Introduction

Since the discovery of 2-D honeycomb lattice of mono-layer carbon atoms called graphene [1], more research interest has been focus toward the 2-D materials. 2-D materials has been considered as a potential candidate in nano-electronics because of its unique physical and chemical properties such as high electron mobility and inherent mechanical strength [2–10]. Nanocomposites consisting of nanoparticles (NPs) or nanocrystals embedded in a matrix have been the subject of many studies motivated by the extraordinary properties obtained in comparison to their single phase [11–18]. A significant advances have been made in designing of mono-layer structures such as boron nitride (BN) and transition metal dichalcogenides such as MoSe, MoS, WS_2, WSe_2, and $NbSe_2$ [19–25]. There are many potential applications for monolayer semiconductors. For example, layered hexagonal BN is used as a dielectric for graphene electronics [26] Likewise, MoS_2 exhibits a direct optical band gap that has been intensively investigated for photovoltaic applications and other electronics devices [26]. Recently, Li et al. [27] designed a two dimensional (2D) inorganic material, namely Be_2C monolayer, by comprehensive density functional theory (DFT) computations. In the designed monolayer, each carbon atom binds to six Be atoms in an almost planar fashion, forming a quasi-planar hexa coordinate carbon (phC) equally. To investigate the potential application of the designed monolayer, Li et al. studied the electrical properties of the Be_2C monolayer using the plane-wave technique implemented in Vienna ab initio simulation package (VASP), where, a direct

✉ Shahram Solaymani
shahram22s2000@yahoo.com

[1] Department of Physics, Kermanshah Branch, Islamic Azad University, Kermanshah, Iran

[2] New Technologies - Research Center, University of West Bohemia, Univerzitni 8, 30614 Pilsen, Czech Republic

[3] Center of Excellence Geopolymer and Green Technology, School of Material Engineering, University Malaysia Perlis, 01007 Kangar, Perlis, Malaysia

[4] Department of Physics, Pachhunga University College, Aizawl, 796001, India

[5] Department of Physics, North Tehran Branch, Islamic Azad University, Tehran, Iran

[6] Department of Physics, Science and Research Branch, Islamic Azad University, Tehran, Iran

Published online: 04 April 2018

gap of about 1.52 eV has been observed. However, they recalculated the band structure of Be_2C monolayer using the hybrid HSE06 functional and predicted a 2.34 eV direct band gap. As a semiconductor with a direct medium band gap, Be_2C monolayer is promising for applications in electronics and optoelectronics [28]. Needless to say, adding impurities play an important role in the potential applications of semiconductors in optoelectronic devices. Without impurities, there would be no diode and no transistor. The control of conductivity of semiconductors enhances their performance in existing applications.

In the present work, the electronic and optical properties of monolayer nano structures Be_2C with Si and Ge impurities have been investigated using density functional theory (DFT) to exploit them as a candidate for optoelectronics devices.

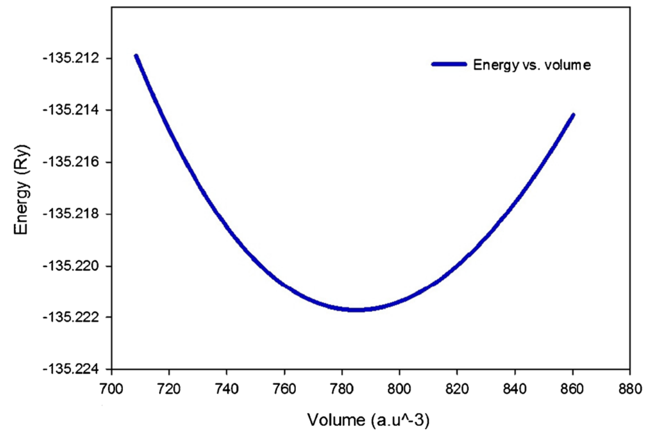

Fig. 2 The unit cell total energy versus the unit cell volume for Be_2C nanosheet. The volume unit is given in $(bohr)^{1/3}$

2 Computational Details

The all-electron full potential linear augmented plane wave (FP-LAPW+lo) method in a scalar relativistic version as embodied in the Wien2k code [29] was used to calculate the electronic properties of Be_2C and Si, Ge doped Be_2C monolayer. The generalized gradient approximation (PBE-GGA) [30] was employed to describe the exchange and correlation energies. In the presented calculation, for isolating the Be_2C layer a supercell including 27 atoms was generated and to avoid neighboring layers interactions, vacuum layer of 15 angstrom in non-periodic direction is considered. Based on Mankhorest approximation, special k points were generated with grid 7*7*1, while RKmax, Gmax and lmax were set to 7, 14 and 10 respectively. Needless to say that RKmax refers to the product of the smallest atomic sphere radius R_{MT} times the largest K-vector K_{max}, Gmax is the magnitude of the largest K-vector in the Fourier expansion of rho and V and lmax lmax is the maximum value of l (angular momentum) for the (l,m) expansion of wave function or density. Also the relaxation process was continued until the charge was converged to be 0.0001e as well as the maximum force on each atom was less 1 mRyd/au.

3 Results and Discussions

3.1 Structural Properties of the Be_2C Monolayer

In this work, to obtain an optimized structure, the unit cell volume was optimize. The volume optimization done using

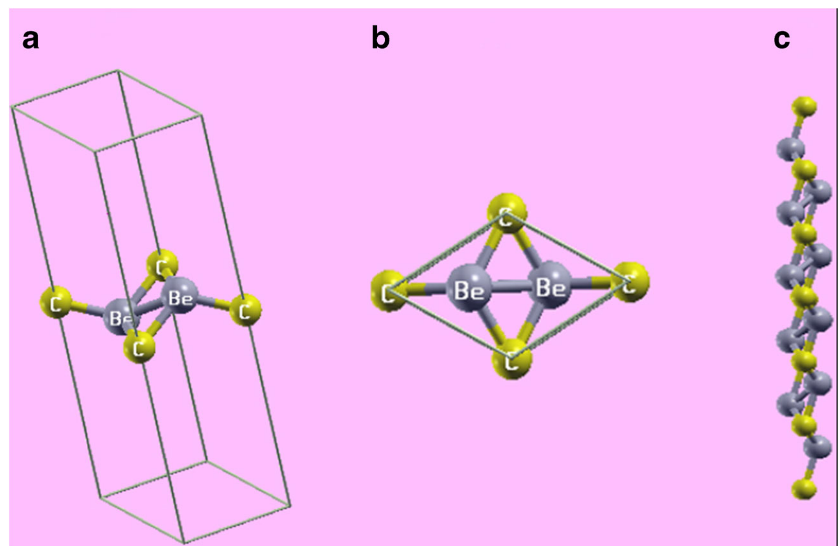

Fig. 1 **a** The optimized structure of the Be_2C unit cell. **b** The top view of the optimized structure of the Be_2C unit cell. **c** The side view of the optimized structure of the Be_2C unit cell. The gray and yellow, balls indicate the C and Be atoms respectively

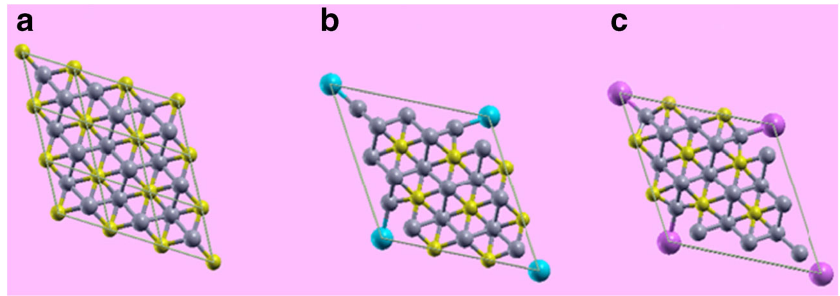

Fig. 3 **a** The optimized structure of the Be_2C. **b** The optimized structure of the Be_2C:Si. **c** The optimized structure of the Be_2C:Ge. The gray, yellow, blue and pink balls indicate the Be, C, Si and Ge atoms respectively

Murnaghan's fitting based on Birch-Murnaghan equation [31]:

$$E(V) = E_0 + \frac{9B_0V_0}{16}\left\{\left[\left(\frac{V_0}{V}\right)^{\frac{2}{3}} - 1\right]^3 B_0'\right\} + \frac{9B_0V_0}{16}\left\{\left[\left(\frac{V_0}{V}\right)^{\frac{2}{3}} - 1\right]^2 \left[6 - \left(\frac{V_0}{V}\right)^{\frac{2}{3}}\right]\right\}, \quad (1)$$

The energy vs. volume was calculated and the optimized lattice parameters are obtained. In which V_0 is the initial considered volume, V is the deformed volume, B_0 is the bulk modulus, and $B^{/}0$ is the derivative of the bulk modulus with respect to pressure. The minimum point of the E-V curve provides the equilibrium lattice constant of the crystal cell.

Using this procedure, the optimized lattice constant of 3 angstrom is achieved which is in a good agreement with the previous reported data [28]. The optimized structure of the Be_2C monolayer unit cell from top and side views is shown in Fig. 1a–c, where a unit cell of the monolayer consists of two Be atoms and one C atoms, where, every two neighboring Be atoms in Be_2C monolayer are buckled into two different atomic planes, 0.46 angstrom above and below the C atomic plane, respectively. The atomic positions of graphene-like structure of Be_2C monolayer are considered as Be(0,0,0.5306), Be(0.666,0.333,0.0.4693) Be and C(0.333,0.666,0.5), where, every two neighboring Be atoms in Be_2C monolayer are buckled into two different atomic planes, 0.46 above and below the C atomic plane, respectively. The graph of total energy of Be_2C unit cell versus volume is presented in Fig. 2.

In continuation, the structure was relaxed to obtain a force optimized (3×3) super-cell with minimum exerting force between any two atoms. The calculated Be-C and Be-Be bond lengths is about 1.79 angstrom and 1.96 angstrom. The stability of Be_2C monolayer was confirmed by the cohesive energy calculation. According to the definition of cohesive energy,

$$E_C = \frac{\left[N_C E_C^{Single} + N_{Be} E_{Be}^{Single}\right] - E_{total}^{Be_2C-sheet}}{N_C + N_{Be}}, \quad (2)$$

where $E_{total}^{Be_2C-sheet}$ is the total energy of any sheet, E_X^{Single} and N_X (X= Be, C) are the energy and number of the single

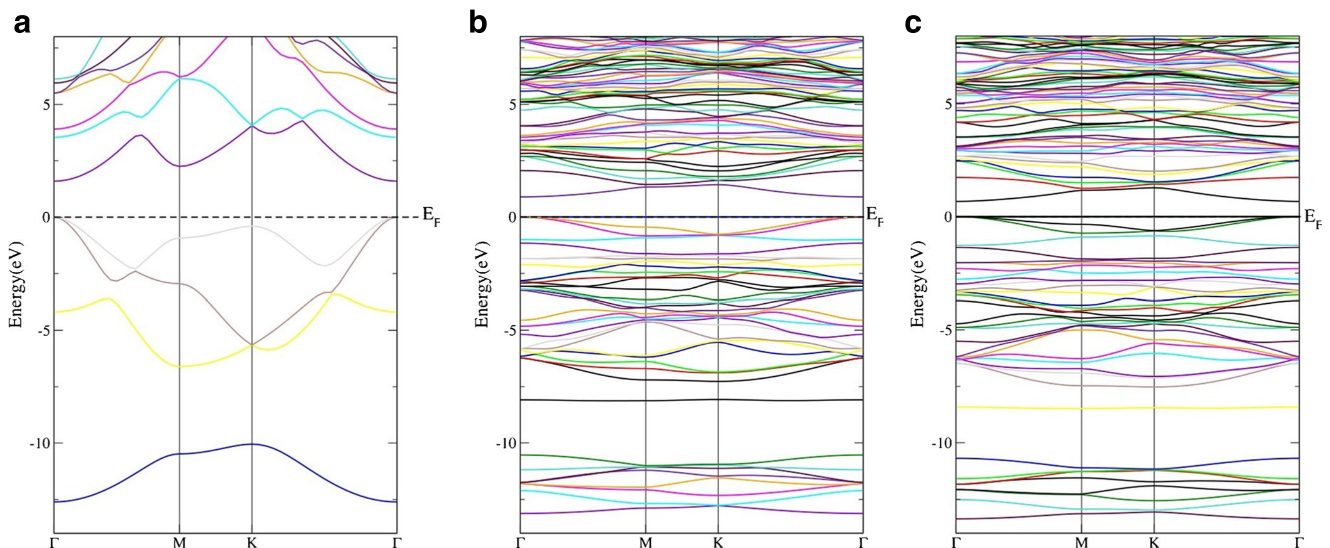

Fig. 4 **a** The band diagram of the Be_2C. **b** The band diagram of the Be_2C:Si. **c** The band diagram of the Be_2C: Ge

X atoms, respectively [32]. From this point of view the positive sign of the cohesive energy means that the structure is stable. Our computations show that Be_2C monolayer has a cohesive energy of about 5.33 eV/atom, which is good evidence that the structure is stable. Afterwards, the Be_2C monolayer has been considered and the band diagram of the sheet was plotted, a direct gap of around 1.6 eV is obtained along the Γ point (Γ is center of first brillouin zone). Therefore the calculated results are in good agreement with previous work [28].

In continue the electronic properties of Be_2C sheet with Si and Ge impurities have been investigated to exploit them in optoelectronics devices. The two doped Be_2C monolayers have been optimized by force and charge converging. For estimation of the structural stability of the designed Si doped and Ge doped Be_2C sheets, the cohesive energy of the two structures have been calculated by subtracting the average energy of the atoms of the system from the average energy of the isolated atoms constructing a sample. Form this point of view the positive sign of the cohesive energy means that the structure is stable. The cohesive energies of 5.186 eV/atom and 5.197 eV/atom has been calculated for the Si doped and Ge doped structures respectively, that means the mentioned structures are stable. The optimized

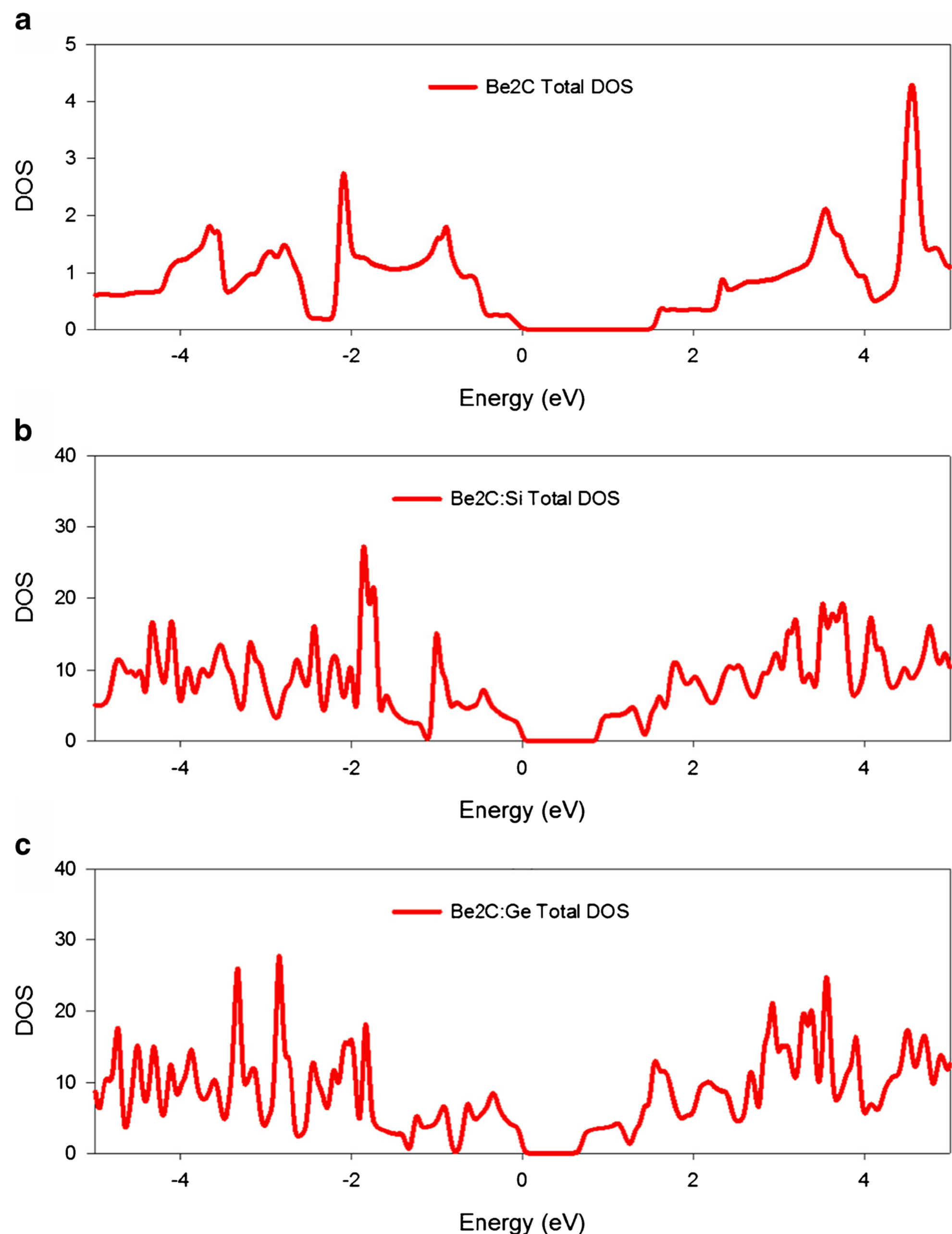

Fig. 5 The total electronic density of states for the **a** Be_2C, **b** Be_2C:Si and **c** Be_2C:Ge

structure of the Be_2C, Be_2C:Si and Be_2C:Ge sheets are illustrated in Fig. 3a–c.

3.2 Electrical Band Structure and Density of States

To investigate the electronic properties of Si and Ge doped Be_2C monolayer, the energy bands diagram has been plotted for the Be_2C monolayer and also for two doped compounds. The band diagram for Be_2C, Be_2C:Si and Be_2C:Ge monolayers are illustrated in Fig. 4a–c, respectively. According to Fig. 4a–c direct band gaps of about 1.59, 0.89 eV and 0.67 eV appears in Be_2C, Be_2C:Si and Be_2C:Ge band structures respectively. It can be seen that similar to the Be_2C sheet, for the Si doped and Ge doped Be_2C sheet the band gap located at the Γ point. Additionally, as the atomic number of the impurity increases, the band gap reduction is increased. Considering the valance electrons of the carbon, silicon and germanium atoms set as $2s^22p^2$, $3s^23p^2$ and $4s^24p^2$, it can be seen that by doping impurities in carbon site, no fundamental changes in band structures can be expected, which is confirmed by the band structure diagrams, where, from -14 eV to -10 eV, the electronics levels are occupied by core electrons. Then the direct band gaps separate the valance electron from conducting electrons. By close inspection of the band diagrams, it can be observed that for the both doped cases, a new electronics level has been appeared in about -8.5 eV in band structures and the band curves have become relatively flat near the Fermi level which implies that the effective mass is high with low mobility. Comparing with the Be_2C monolayer in the doped sheets, a perturbation potential originated by additional density of electrons appeared which forces the electronics states. In addition, the electronic density of states of the two compounds are plotted. The total density of states for the Be_2C, Be_2C:Si and Be_2C:Ge sheets are plotted in Fig. 5a, b and c respectively. Considering Fig. 3a–c, one can find that the two doped compounds remain p-type semiconductor with energy band gaps of the about 0.89 eV and 0.67 eV. The partial density of sates for Be_2C:Si and Be_2C:Ge compounds are illustrated in Fig. 6.

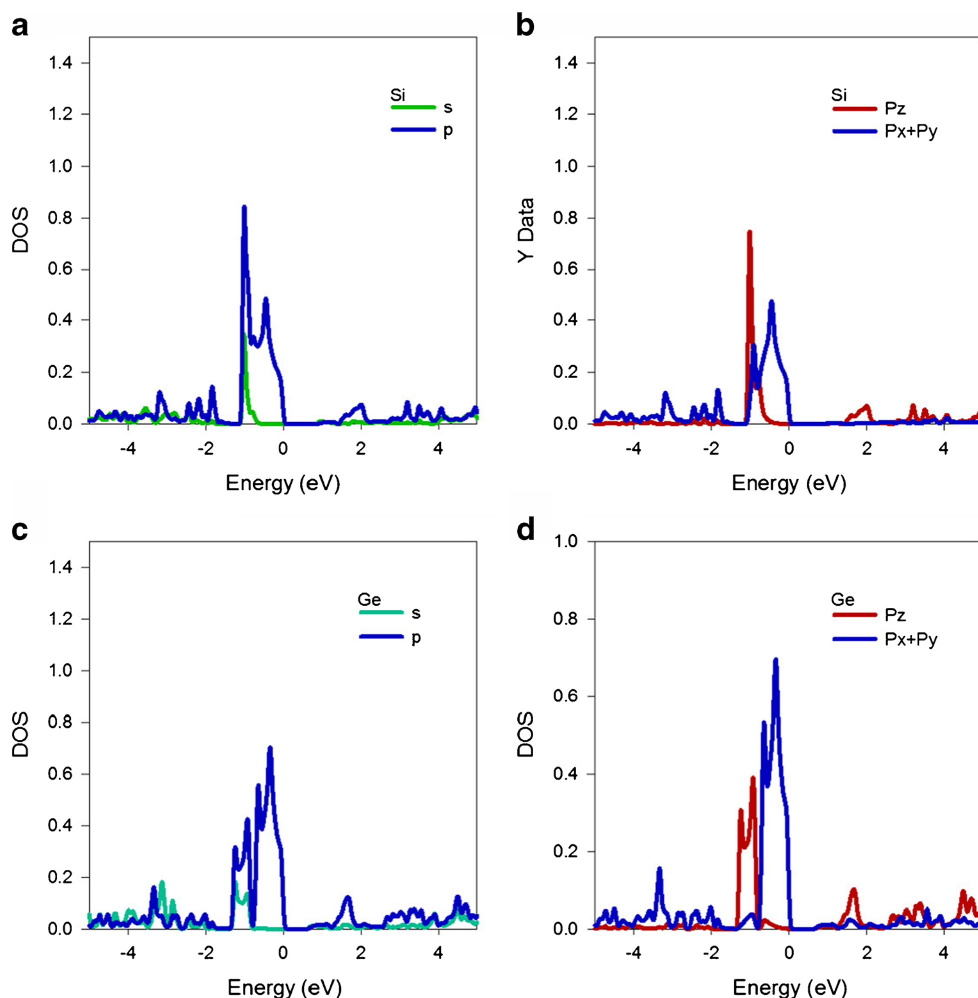

Fig. 6 The partial density of states for the **a** s and p orbitals of Si atom in Be_2C:Si, **b** P_z and P_x+P_y orbitals of Si atom in Be_2C:Si **c** s and p orbitals of Ge atom in Be_2C:Ge, **d** P_z and $P_x + P_y$ orbitals of Ge atom in Be_2C:Ge

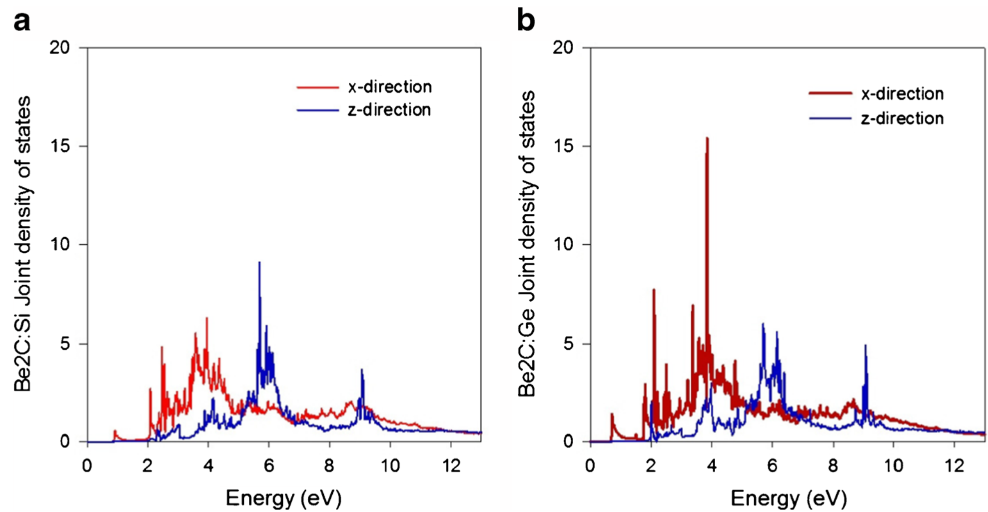

Fig. 7 The Joint density of states for **a** Be_2C:Si and **b** Be_2C:Ge monolayer

3.3 Optical Properties

In this section, the optical properties of the two proposed monolayer compounds are calculated and discussed in details. At first, the optical inter-band transitions of the materials can be investigated by considering the joint density of states which indicates the electrons that contribute in optical transition. The joint density of states

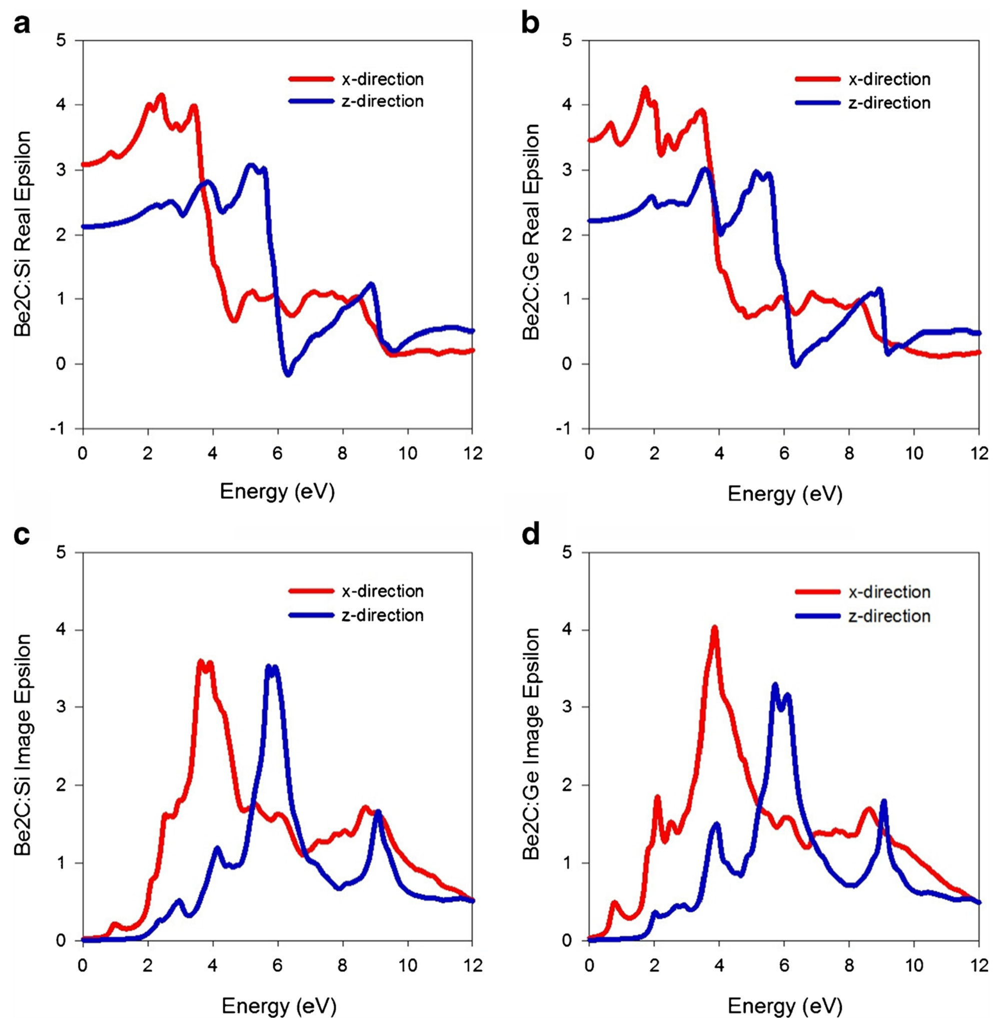

Fig. 8 The real and imaginary parts of the complex dielectric function of Be_2C:Si (**a** and **b**) and Be_2C:Ge monolayer (**c** and **d**)

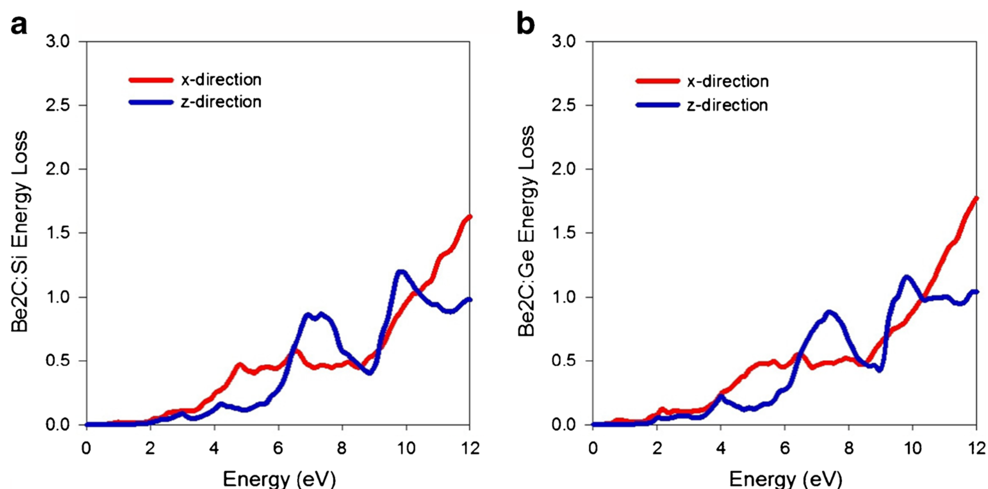

Fig. 9 The energy loss function of **a** Be_2C:Si and **b** Be_2C:Ge

for two doped mono-layers for both x and z directions are plotted in Fig. 7a and Fig. 7a. Considering the Fig. 7a–b, one can see that the two compounds indicate anisotropic behaviors in xx- and zz-polarization directions, where, in xx-polarization direction the local peaks in joint density of states which determine the electron transitions are occurred in around 0.89 eV, 2.04 eV, 2.47 eV, 3.57 eV, 3.92 eV and 4.33 eV for Be_2C:Si nanosheet, while in zz-polarization direction the local peaks are occurred in 2.2 eV, 2.9 eV, 4.1 eV, 5.6 eV, 5.9 eV and 9.1 eV. A similar behavior

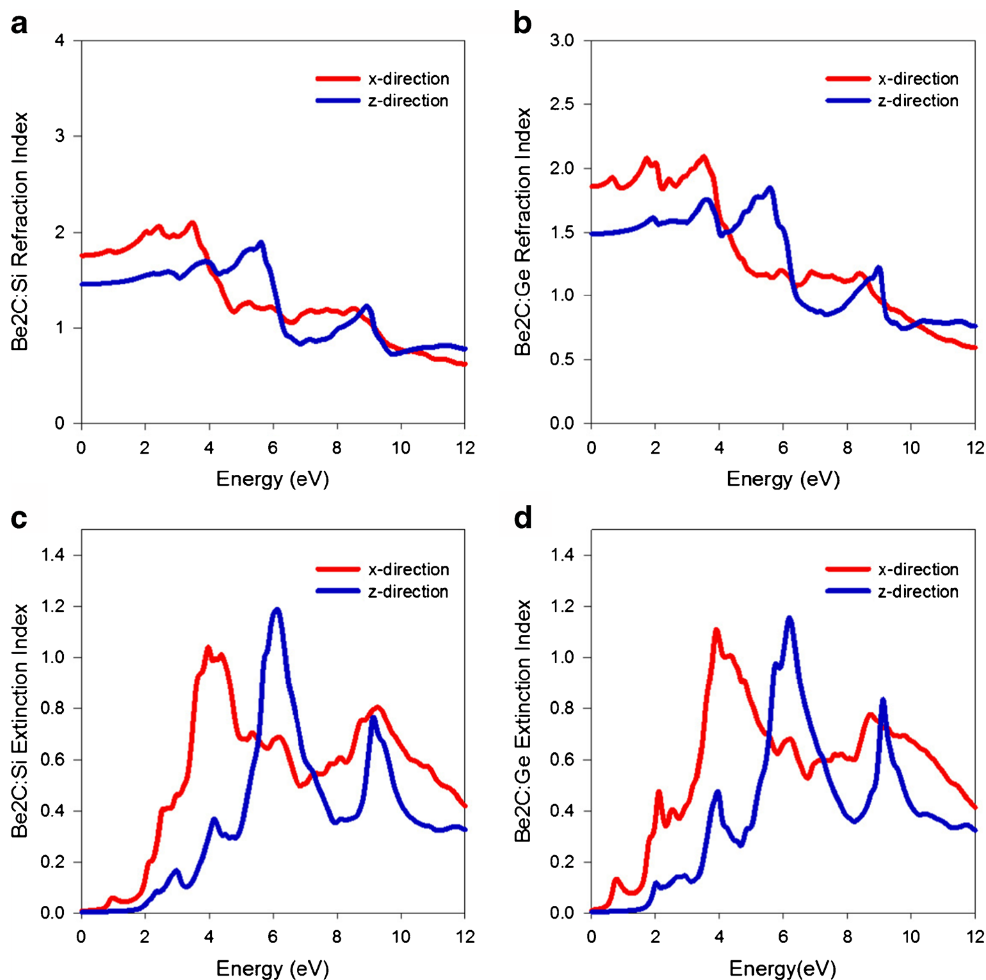

Fig. 10 The refractive index of the **a** Be_2C:Si and **b** Be_2C:Ge monolayer. The extinction index of the **c** Be_2C:Si and **d** Be_2C:Ge monolayer

is shown by Be_2C:Ge, where, in xx-polarization direction the local peaks are occurred in around 0.67 eV, 1.7 eV, 2.1 eV, 2.4 eV, 3.4 eV, 3.8 eV and 4.7 eV for Be_2C:Ge nanosheet, while in zz-polarization direction the local peaks are occurred in 2 eV, 4 eV, 5.67 eV, 6.1 eV, 6.3 eV. The first main peaks corresponding exactly to the energy band gaps located in Γ direction occur in 0.67 eV and 0.89 eV for Si doped and Ge doped compounds respectively, this tow peaks in x-polarization direction are originated by the transition from the valance band maximum (VBM) to the conduction band minimum (CBM). The linear optical response of the material to an incoming electromagnetic field is determined by the dielectric function. In general, the dielectric function is a complex-valued function which is defined as:

$$\varepsilon(\omega) = \varepsilon_R(\omega) + i\varepsilon_I(\omega). \quad (3)$$

Where, $\varepsilon_R(\omega)$ and $\varepsilon_I(\omega)$ represent the real and imaginary parts of the complex dielectric function. The imaginary part of the function can be obtained as follows:

$$\varepsilon_I(\omega) = \frac{h^2 e^2}{\pi m^2 \omega^2} \sum\nolimits_n \int d_k \langle \psi_k^{C_n} | P^\alpha | \psi_k^{V_n} \rangle \langle \psi_k^{v_n} | P^\beta | \psi_k^{c_n} \rangle \delta\left(E_k^{c_n} - E_k^{V_n} - \omega\right), \quad (4)$$

where $P^{\alpha(\beta)}$ is the dipole matrix, v_n and c_n are the initial and final states, respectively. Using the Kramers-Kroning relation, the real part of the dielectric function can be extracted from the imaginary part [33].

$$\varepsilon_R(\omega) = \delta_{\alpha\beta} + \frac{2}{\pi} P \int_0^\propto \frac{\omega \varepsilon_I(\omega)}{\omega^2 - \omega^{2'}} \quad (5)$$

Where P denotes the Cauchy principal value. The real part of the dielectric function is related to polarization and anomalous dispersion, while the imaginary part describes the dissipation of energy into the material [33]. The refractive index $n(\omega)$, the extinction coefficient $k(\omega)$, electron energy loss function $L(\omega)$, the reflectivity $R(\omega)$, and the absorption coefficient $\alpha(\omega)$ can be calculated in

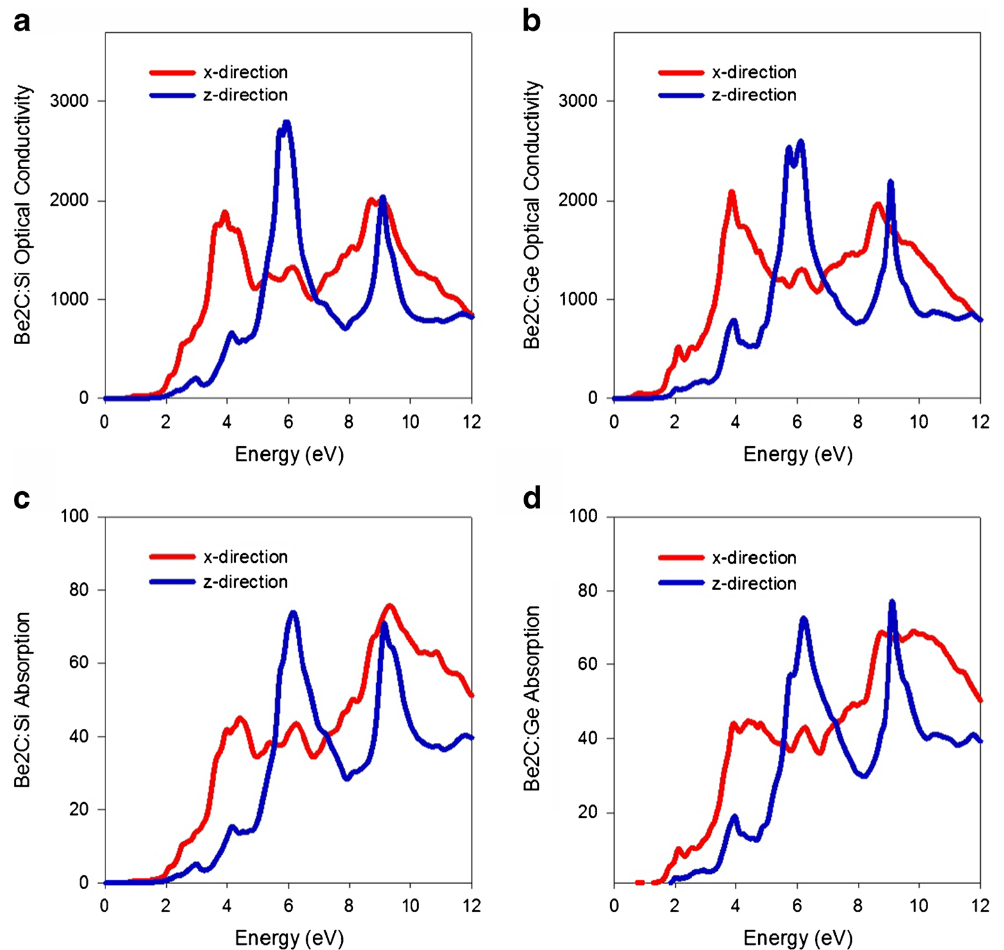

Fig. 11 The optical conductivity and absorption coefficient of Be_2C: Si and Be_2C: Ge

terms of the real and imaginary part of the complex optical permittivity as follows:

$$n(\omega) = \frac{\left(\varepsilon_I + \left(\varepsilon_I^2 + \varepsilon_R^2\right)^{1/2}\right)^{1/2}}{\sqrt{2}}, \quad (6)$$

$$k(\omega) = \frac{\left(-\varepsilon_I + \left(\varepsilon_I^2 + \varepsilon_R^2\right)^{1/2}\right)^{1/2}}{\sqrt{2}}, \quad (7)$$

$$L(\omega) = \frac{\varepsilon(\omega)}{\varepsilon_I^2(\omega) + \varepsilon_R^2(\omega)}, \quad (8)$$

$$R(\omega) = \left|\frac{\sqrt{\varepsilon(\omega)} - 1}{\sqrt{\varepsilon(\omega)} + 1}\right|^2, \quad (9)$$

$$\alpha(\omega) = \sqrt{2}\omega\left(\left[\varepsilon_I^2 + \varepsilon_R^2\right]^{1/2} - \varepsilon_I(\omega)\right)^{1/2}, \quad (10)$$

The real and imaginary parts of the complex dielectric function of Be_2C:Si and Be_2C:Ge are shown in Fig. 8a–d. It can be seen that the real part of the function exhibits a considerable anisotropy between the components. The static value of the real? in x- and z-polarization direction is about 3.1 and 2.1 for Be_2C:Si compound, while it is around 3.5 and 2.3 for x- and z-polarization direction for B_2C:Ge compound. The above mentioned values confirm that Be_2C: Si possess larger energy gap than Be_2C: Ge. Also x-polarization direction for both compounds show two peaks in visible region. However in the edge of the ultra violet region, the Real ε decreases rapidly, while for the component along z-polarization direction show rapid decrease at around 5.0 eV. The imaginary part of the complex dielectric function for Be_2C:Si and Be_2C:Ge are shown in Fig. 8b and d, where the absorption edges occurs at around 0.9 eV and 1.5 eV for the components along x- and z-polarization direction of Be_2C:Si compound whereas for Be_2C:Ge compound it occurs at around 0.7 eV and 1.4 eV. The fundamental peaks are situated at around 3.0 eV and 6.0 eV for the components along x- and z-polarization direction for Be_2C: Si compound while at around 4.0 eV and 6.0 eV for Be_2C: Ge compound. Also two small peaks appears at around 9.0 eV for both components of Be_2C: Si and Be_2C:Ge.

Figure 9a–b shows the energy loss function of Be_2C: Si and Be_2C: Ge compounds. According to the eloss plots, the energy loss of both compound increased rapidly at around 13.0 eV. It is clear that both compounds illustrate anisotropic behavior in the region below ultra violet region. Also, interestingly, small peaks can be seen in the energy region between 6.0-11.0 eV which confirms the presence of plasmons.

Another optical property which is important to be considered is refractive index. The refractive index determines how much light is bent, or refracted, when entering a material. The real part and imaginary part of the refractive index of the Be_2C:Si and Be_2C:Ge monolayer are illustrated in Fig. 10a, d. The real part of the refractive index confirms nonmetal behavior of the material in both x and z directions. By looking at the imaginary part of the refractive index, one can see a peak in UV edge for x direction. Also a refraction peak is occurred at around 6.0 eV for z direction.

The optical conductivity and absorption coefficient of Be_2C:Si and Be_2C:Ge compounds are shown in Fig. 11a–d. It is clear that there is an optical conduction gap of about 0.9 eV for Be_2C: Si while it is about 0.7 eV for Be_2C: Ge. It has been noticed that the maximum optical conductivity of components along x- and z-polarization directions occurs in visible and UV regions respectively. Furthermore, the absorption coefficient graph confirms the electronic band gap in both directions.

4 Conclusion

In summary, by considering a supercell method 27 atoms of Be_2C have been generated. A first principle calculation within FP-LAPW method has been implemented to investigate the electronic and optical properties of pure and Si/Ge doped layered Be_2C. The structure stability was checked by using Cohesive energy calculation, which predicts the Si and Ge doped Be_2C monolayer have stable structures. The doping of Si/Ge has modified the electronic band structures of Be_2C, consequently a band gap. On doping Si and Ge impurities the energy band gap of Be_2C monolayer is reduced from 1.54 eV to 0.89/0.68 eV for Be_2C:Si/Be_2C:Ge, respectively. The calculated optical properties exhibit the existence of a considerable anisotropy between the two components along x- and z-polarization direction. The calculation indicates that the X (Si, Ge) doped Be_2C monolayer has good potential application in opto-electronics devices.

Acknowledgements It is our pleasure to thank Soheila Gholipour, Yasna Naseri and Viana Naseri for their interests in this work. A. H. Reshak would like to acknowledge the CENTEM project, reg. no. CZ.1.05/2.1.00/03.0088, cofounded by the ERDF as part of the Ministry of Education, Youth and Sports OP RDI programme and, in the follow-up sustainability stage, supported through CENTEM PLUS (LO1402) by financial means from the Ministry of Education, Youth and Sports under the National Sustainability Programme I. Computational resources were provided by Meta Centrum (LM2010005) and CERIT-SC (CZ.1.05/3.2.00/References08.0144) infrastructures.

Compliance with Ethical Standards

Conflict of interests The authors report no conflict of interests. The authors alone are responsible for the content and writing of the paper.

References

1. Nakada K et al (1996) Phys Rev B 54:17954
2. Okada S (2008) Phys Rev B 77:041408
3. Novoselov KS et al (2005) Nature 438:197
4. Su C, Jiang H, Feng J (2013) Phys Rev B 87:075453
5. Mukhopadhyay C, Behera H (2013) World J Eng 10:39–43
6. Zhu J et al (2014) Small 10:3480
7. Matte R et al (2010) Angew Chem Int Ed 49:4059–4062
8. Radisavljevic B et al (2011) Nat Nanotechnol 6:147–150
9. Nag A et al (2010) ACS Nano 4:1539–1544
10. Zhang X et al (2014) Mater Res Bull 53(2014):96–101
11. Solaymani S et al (2013) Eur Phys J Appl Phys 64:11301
12. Dalouji V et al (2016) Eur Phys J Plus 131:84
13. Lashgari H et al (2016) Appl Surf Sci 369:76–81
14. Ghodselahi T et al (2012) Eur Phys J D 66:299
15. Solaymani S et al (2012) J Fusion Energ 31:591
16. Arman A et al (2015) J Mater Sci: Mater Electron 26:9630–9639
17. Arman A et al (2015) Prot Met Phys Chem Surf 51:575–578
18. Ţălu S et al (2016) J Microscopy 264:143–152
19. Castro Neto AH et al (2009) Rev Mod Phys 81:109
20. Mak KF et al (2010) Phys Rev Lett 105:136805
21. Chang CH et al (2013) Phys Rev B 88:195420
22. Yun WS et al (2012) Phys Rev B 85:033305
23. Gutierrez HR et al (2013) Nano Lett 13:3447
24. Tonndorf P et al (2013) Opt Express 21:4908
25. Shi H et al (2013) Phys R ev B 87:155304
26. Jang SK et al (2016) Sci Rep 6:30449
27. Li Y et al (2014) Angew Chem Int Ed Engl 53:7248–7252
28. Moon P, Koshino M (2014) Phys Rev B 90:155406
29. Blaha P, Schwarz K, Madesen GK, Kvasnicka D, Luitz J (2001) WIEN2K, an augmented plane wave + local orbitals program for calculating crystal proper-ties. Karlheinz Schwarz Techn; Universitaetwien, Wein
30. Perdew JP et al (1996) Phys Rev let 77:3865
31. Birch F, Geophys J (1978) Res B 83:1257–1268
32. Boochani A et al (2017) J Phys Chem C 121:3978–3986
33. Yu PY, Cardona M (1999) Fundamentals of semiconductors physics and materials properties. Springer, Berlin